Supporting Information

Charge Carrier Mapping for Z-scheme Photocatalytic Water Splitting Sheet by Categorization of Microscopic Time-resolved Image Sequence

Makoto Ebihara[1] Takeshi Ikeda,[2,3] Sayuri Okunaka,[2,3] Hiromasa Tokudome,[2.3] Kazunari Domen,[4,5] and Kenji Katayama[1*]

[1] Department of Applied Chemistry, Chuo University, Tokyo 112-8551, Japan

2 Research Institute, TOTO Ltd., Kanagawa 253-8577, Japan

3 Japan Technological Research Association of Artificial Photosynthetic Chemical Process (ARPChem), Tokyo 101-0032, Japan

4 Research Initiative for Supra-Materials, Interdisciplinary Cluster for Cutting Edge Research, Shinshu University, Nagano 380-8553, Japan

5 Office of University Professors, The University of Tokyo, Tokyo 113-8656, Japan

*Corresponding author:

K. Katayama, Phone: +81-3-3817-1913, E-mail: kkata@kc.chuo-u.ac.jp

The scavenger effect for Rh-doped $SrTiO_3$ (STOR) by methanol (MeOH)

In our experiments, the samples were excited by the pump light with a wavelength of 355 nm (3.55 eV) due to the limitation of our equipment, and it led to the interband transitions for STOR and Mo-doped $BiVO_4$ (BVOM), causing electrons and holes photo-excited directly in the conduction and valence bands. We assumed that the photo-excited holes at the valence band in STOR decayed to the Rh^{3+} state observed as the slow rising component (formation of Rh^{4+} state) until 10 μs in ACN. Since it was reported that the holes at the Rh^{3+} states could be scavenged by MeOH, we measured the response of STOR in MeOH. The result is shown in Fig.S1, and it clearly demonstrated that the slow rising component in ACN was quenched in MeOH. Thus, we concluded that this rising component was attributed to the hole decay process to Rh^{3+} state, corresponding to the oxidation process from Rh^{3+} to Rh^{4+} states in STOR.

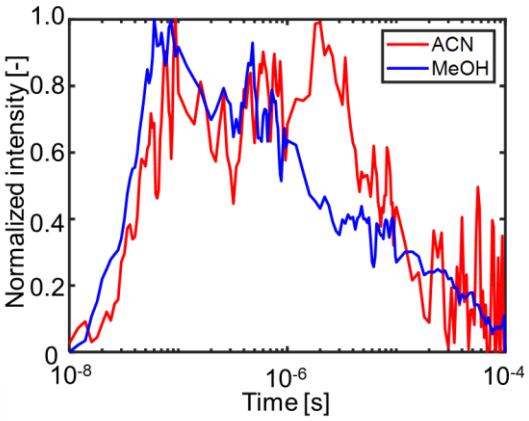

Fig.S1 The refractive index change response of STOR in ACN and MeOH until 100 μs, obtained by the PI-PM image sequence.

The role of ITO binder

It has been reported that the ITO binder, corresponding to the charge transfer mediator, proceeds the recombination between the electrons in oxygen evolution photocatalyst (OEP) and the holes in hydrogen evolution photocatalyst (HEP), and the efficiency of oxygen and hydrogen evolution rate was drastically improved in this system by inserting this in-between. Therefore, we compared two Z-scheme systems with ITO (STOR/ITO/BVOM) and without ITO (STOR/BVOM) to confirm the effect of the ITO binder. Figure S2 compares the responses of the refractive index change for STOR/ITO/BVOM and STOR/BVOM in ACN. From these responses, we could observe a delayed rising component of around 10 μs in STOR/BVOM, and this component was similar to the Rh^{4+} formation for the STOR only in ACN (refer to Fig.S1).

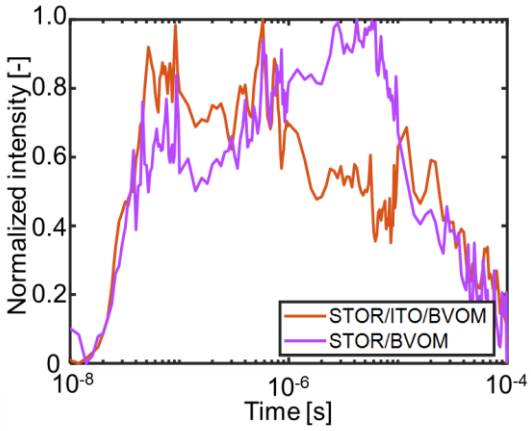

Fig.S2 The comparison of the refractive index change responses between the Z-scheme sample systems with a charge mediator, ITO (STOR/ITO/BVOM) and without it (STOR/BVOM) in ACN until 100 μs, obtained by the PI-PM image sequences.

The difference between these two systems was only the insertion of the ITO binder. Hence, a possible factor for this difference originated from the charge transfer efficiency of electrons in BVOM and the holes in STOR because the recombination between the electrons in OEP and the holes in HEP was retarded, and they remained in each material without the ITO binder. Moreover, judging from the similarity in the responses between the STOR/BVOM and the STOR only, the rising component observed in STOR/BVOM must be related to the hole accumulation to the Rh^{3+} state (Rh^{4+} formation) in STOR. This component can possibly be scavenged by a hole scavenger (MeOH) if this assumption is correct. Figure S3 shows the refractive index change response for the STOR/BVOM system in ACN (inert solvent) and MeOH. The result clearly showed that the slow rising component until 10 μs in STOR/BVOM in ACN disappeared in MeOH, and instead, the faster-rising response

until 1 μs showed up, which was similar to that of STOR/ITO/BVOM in ACN. It is supposed that MeOH worked to reduce the Rh^{4+} state, instead that the electrons in BVOM were used to reduce it with an ITO binder. These facts verified that the ITO mediator worked to prevent the increase in the Rh^{4+} states in STOR and proceed the water-splitting reaction efficiently.

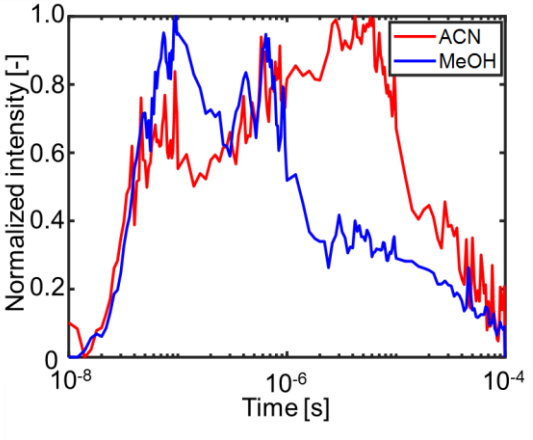

Fig.S3 The refractive index change responses for the Z-scheme system (STOR/BVOM) without the ITO binder in ACN (red) and MeOH (blue) until 100 μs, obtained by the PI-PM image sequences.

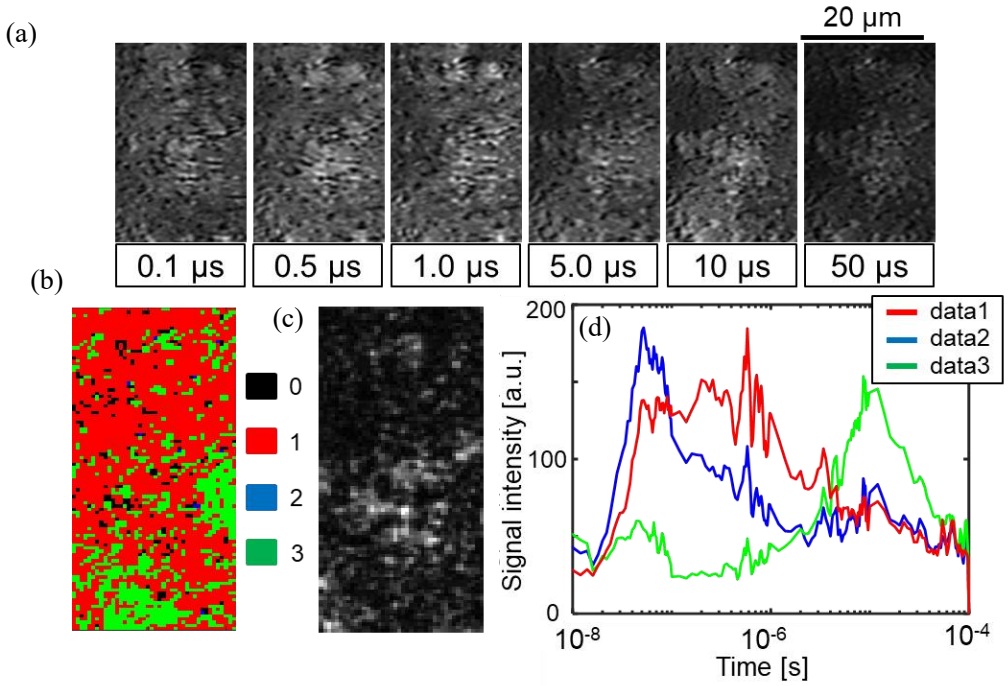

Fig. S4 (a) An image sequence of the refractive index response for STOR/ITO/BVOM in ACN in a square region (20×50 μm) corresponding to No.2 in Fig.1(c) on the order from nanoseconds to microseconds. The scale bar corresponds to 20 μm. (b) The categorized mapping of the charge carrier responses of (a). An outlier positioned far from all categories were colored in black (#0). (c) A microscopic image in the same area as (a). (d) The averaged responses for each category in (b) are shown.

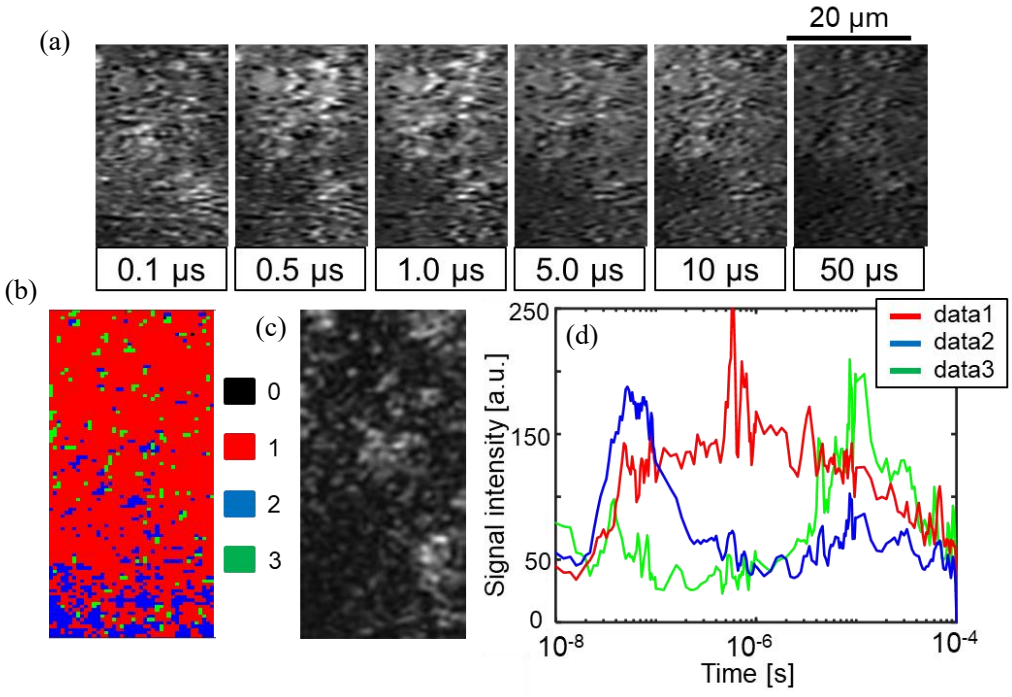

Fig. S5 (a) An image sequence of the refractive index response for STOR/ITO/BVOM in ACN in a square region (20×50 μm) corresponding to the region No.3 in Fig.1(c) on the order from nanoseconds to microseconds. The scale bar corresponds to 20 μm. (b) The categorized mapping of the charge carrier responses of (a). An outlier positioned far from all categories were colored in black (#0). (c) A microscopic image in the same area as (a). (d) The averaged responses for each category in (b) are shown.

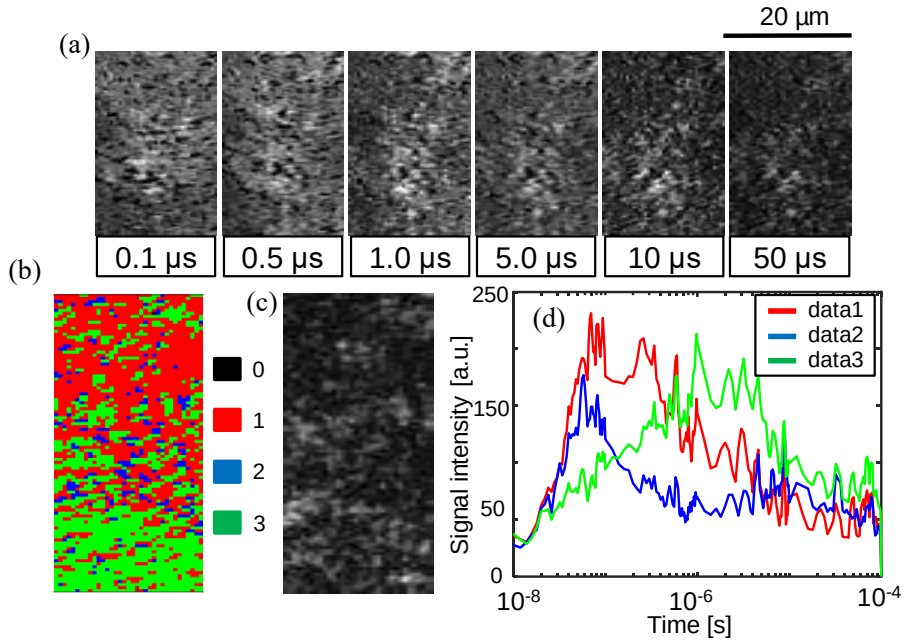

Fig. S6 (a) An image sequence of the refractive index response for STOR/ITO/BVOM in ACN in a square region (18×50 µm) corresponding to the region No.4 in Fig.1(c) on the order from nanoseconds to microseconds. The scale bar corresponds to 20 µm. (b) The categorized mapping of the charge carrier responses of (a). An outlier positioned far from all categories were colored in black (#0). (c) A microscopic image in the same area as (a). (d) The averaged responses for each category in (b) are shown.

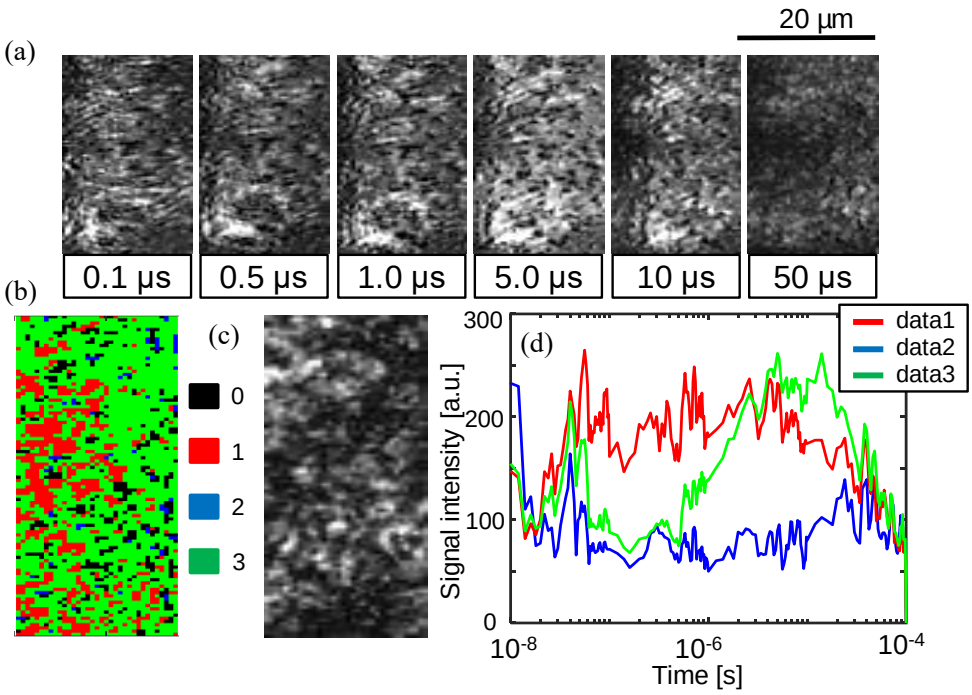

Fig. S7 (a) An image sequence of the refractive index response for STOR/BVOM in ACN in a square region (18×50 µm) corresponding to No.2 in Fig.1(c) on the order from nanoseconds to microseconds. The scale bar corresponds to 20 µm. (b) The categorized mapping of the charge carrier responses of (a). An outlier positioned far from all categories were colored in black (#0). (c) A microscopic image at the same area as (a). (d) The averaged responses for each category in (b) are shown.

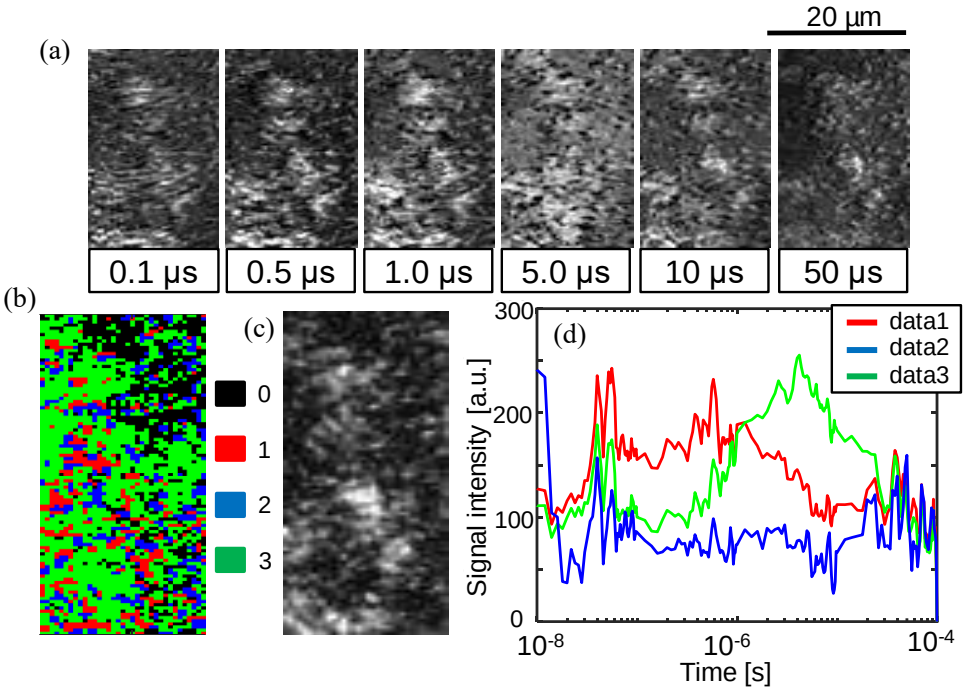

Fig. S8 (a) An image sequence of the refractive index response for STOR/BVOM in ACN in a square region (18×50 μm) corresponding to the region No.3 in Fig.1(c) on the order from nanoseconds to microseconds. The scale bar corresponds to 20 μm. (b) The categorized mapping of the charge carrier responses of (a). An outlier positioned far from all categories were colored in black (#0). (c) A microscopic image in the same area as (a). (d) The averaged responses for each category in (b) are shown.

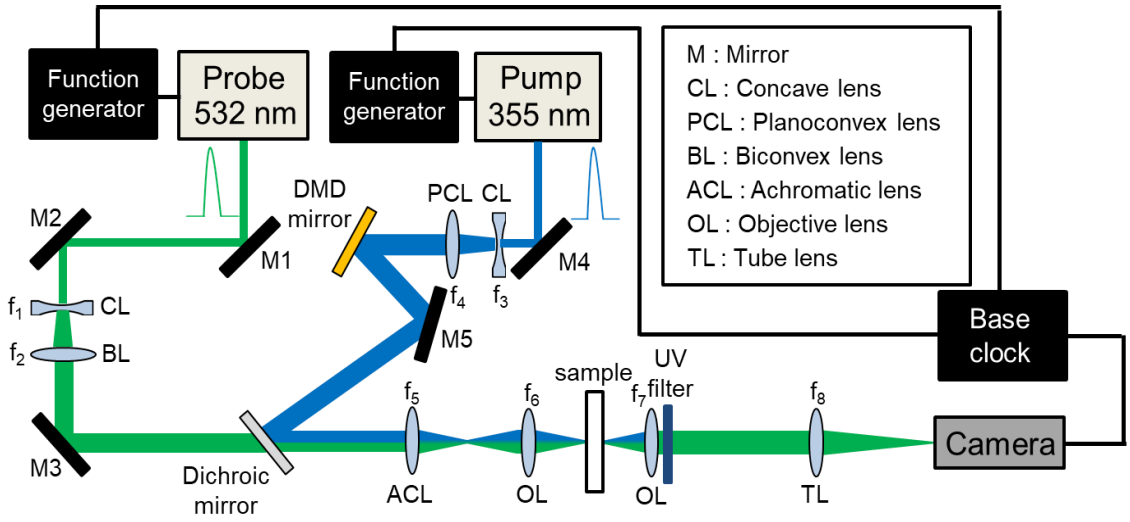

Fig. S9 The schematic overview of the optical setup of patterned-illumination time-resolved phase microscopy (PI-PM). For the pattern illumination, a digital micromirror device (DMD) (Light Crafter 4500, Texas Instruments) was used. The pump light was reflected at the DMD mirror to change the intensity pattern the same as the pattern on a computer. The image of the DMD mirror was relayed with a lens (f = 100 mm) and an objective lens (LUCPLFLN20x, Olympus) to irradiate the same pattern reduced in size (1/14) onto a sample. The pulsed illumination light was collimated with the pump light at the dichroic mirror and illuminated onto a sample. The transmitted light was imaged by an objective lens (LUCPLFLN20x, Olympus) and a tube lens (TTL180-A. Thorlabs). A CMOS camera (MV1-D1024E-160, Photon Focus) had a sensor area of 10.9x10.9mm (1024x1024 pixel), and the central region in the vertical direction (200x1024 pixel) was recorded to reduce the burden of the computer processing. The diameter of the irradiated area by the pump pulse was 0.5 mm. A sequence of images was stored in a computer by varying the time delay between the pump and probe pulse. The time resolution was limited only by the pulse width of the pump and probe lights, 5 ns. The pump light was the third harmonics of a Nd:YAG pulse laser (pulse width: 5 ns, wavelength: 355 nm) (GAIA, Rayture Systems). The probe light was the second harmonics of an Nd:YAG pulse laser (pulse width: 5 ns, wavelength: 532 nm) (GAIA, Rayture Systems). The timing of these pulses was controlled by two function generators (WF1968, NF) triggered by a base clock (DF1906, NF). Each function generator controlled both the timing of the flash lamp and the Q-switch with a time resolution of 100 ps. The pump light intensity was 2.23 mJ/pulse, and the probe light intensity was 0.02 mJ/pulse, respectively.

Preparation of photocatalyst sheets

Printed photocatalyst sheets were prepared as follows. Photocatalysts used, Rh-doped $SrTiO_3$ (Rh/(Rh+Ti) = 4 mol%) and Mo-doped $BiVO_4$ (Mo/(Mo+V) = 0.05 mol%), were prepared by the previous methods.[R1,R2] ITO nanoparticles (ca. 20 nm) were purchased from Koshin Chemical. $SrTiO_3$:Rh, $BiVO_4$:Mo, and ITO were dispersed at a 2:2:1 mass ratio in the organic medium (α-terpineol: 2-(2-butoxyethoxy)ethanol: SPB-TE1 = 4:10:2 (mass ratio). The mass ratio of the powder mixture to the organic medium was 1:19. Then the resulting paste was coated onto a glass substrate by screen-printing using a metal mask (60 μm thick), and finally calcined in air at 573 K for 30 min. The film thickness was approximately 1 μm.

(R1) Konta, R.; Ishii, T.; Kato, H.; Kudo, A. Photocatalytic Activities of Noble Metal Ion Doped SrTiO3 under Visible Light Irradiation. *J. Phys. Chem. B* **2004**, *108* (26), 8992–8995. https://doi.org/10.1021/jp049556p.

(R2) Iwase, A.; Kudo, A. Photoelectrochemical Water Splitting Using Visible-Light-Responsive BiVO4 Fine Particles Prepared in an Aqueous Acetic Acid Solution. *J. Mater. Chem.* **2010**, *20* (35), 7536–7542. https://doi.org/10.1039/C0JM00961J.

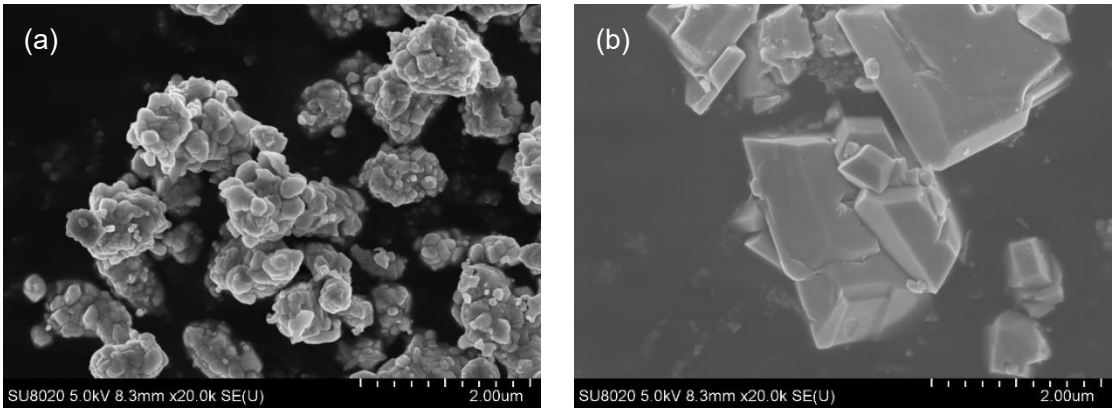

Fig.S10 SEM images of (a) STOR and (b) BVOM. The average diameters of particles were 300 nm and 2 μm, respectively.

163

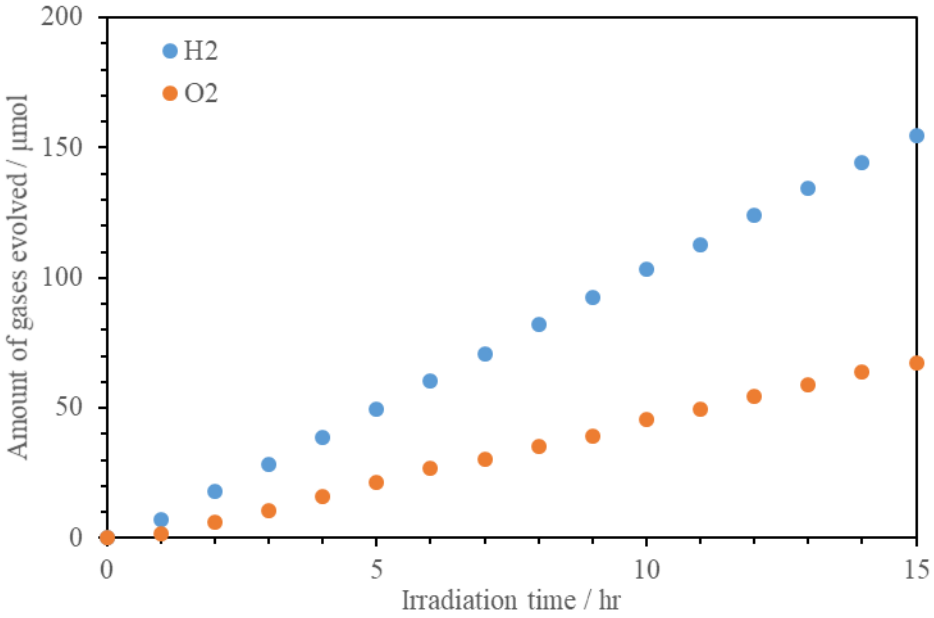

164 Fig.S11 Time courses of amounts of gas evolution on a photocatalyst sheet under visible light
165 irradiation. Sheet size, 2.5 × 2.5 cm; reactant solution, 40 mL of pure water at 288 K; reaction cell,
166 top-irradiated separable cell; light source, 300 W Xe lamp with cut-off filters (λ > 410 nm) .
167